MECHANISM AND PREDICTION OF LASER WET CLEANING OF MARBLE ENCRUSTATION

Paper # P514

Jie Zhang[1], Andrew J. Birnbaum[1], Y. Lawrence Yao[1], Fen Xu[2], John R. Lombard[2]

[1] Department of Mechanical Engineering, Columbia University, New York, NY 10027, USA
[2]Department of Chemistry, City College of New York, New York, NY 10031, USA

Abstract

During the removal of encrustation from marble with 355 nm laser pulses, the effects of the thin liquid layer covering the encrustation are experimentally and numerically investigated. The working mechanism of the liquid layer is analyzed. A two-dimensional axi-symmetric model is proposed to simulate the changes of the temperature, liquid volumetric fraction and vapor pressure in the irradiated encrustation. To model the conservation of mass, momentum, and energy, three coupled nonlinear PDEs are numerically solved. The measured porosity of the encrustation is incorporated into the model. Marble cleaning with three different liquids has different thermodynamic properties, that is, distilled water, ethanol and acetone, are compared in terms of the cleaning efficiency at different fluence levels. With the liquid layer, the surface color of cleaned marble is also studied. In addition, Surface-enhanced Raman spectroscopy (SERS) and the Chromameter are used to identify the chemical constituents and measure the color of the cleaned marble, respectively.

Introduction

The artifacts or buildings, made of natural stones such as marble, are inevitably and gradually covered by a thin layer of black encrustation. The black encrustation has to be removed since it facilitates the degradation of the stone and also extremely decreases the aesthetic value of the stone. At present, chemical cleaning and mechanical cleaning are widely used to remove the encrustation. Due to the possible environmental pollution and the strong dependence on the operator's techniques, their dominating status is challenged by laser cleaning. Irradiated by the laser pulse, the encrustation can be ablated, but the stone keeps intact after the removal of encrustation because of the large difference in their reflectivity. This characteristic called "self-limiting" is very helpful to implement the safe and accurate stone cleaning.

Since John Asmus first in 1971 proposed to apply pulsed laser in the cleaning of encrustation from marble, the effectiveness of Nd:YAG laser in the restoration of various stoneworks has been verified by the massive investigations [1]. However, there are some disadvantages. Pulsed laser can not succeed in removing the quite thick encrustation. The cleaning efficiency is relatively low because of the low ablation rate. The laser pulse generated high temperature is easy to induce the undesirable thermal side effects, such as red-shift and vitrification, on the cleaned surface [2]. In addition, the stone surface gets severe yellowing after the cleaning with laser at 1064 nm [3], and even the 355 nm laser pulse at low fluence also leads to the yellowing of the stone [4].

Many efforts have been made to investigate the particular contamination removed from microelectronic parts with pulsed lasers. As the dimension of microelectronic parts is constantly shrinking, their tolerance to particle size is also decreasing. Laser steam cleaning has shown great potentials in cleaning of the submicron-sized particles owing to the generated cleaning force much larger than dry cleaning [5-6]. Kim, et al. investigated the physical mechanism of laser steam cleaning. It was proven that the cleaning force comes from the bubble nucleation in the superheated liquid [5]. Lu, et al. proposed one model to calculate the cleaning force generated during the inertial-controlled bubble growth [6].

In the present paper, laser cleaning carried out right after a thin layer of suitable liquid sprayed onto the encrustation is referred to as laser wet cleaning. A black encrustation approximately 500 μm thick was removed from limestone by the Q-switched Nd:YAG laser at 1064 nm with the assistance of distilled water. In the case of a thin encrustation approximately 50 μm thick on limestone, the cleaning rate with water was higher than that without water [7]. The application of water prevented the laser cleaned pliocene sandstone from any thermal side effect. It was speculated that the water significantly cooled down the irradiated volume because of its specific heat 5 times higher than sandstone [3]. The measured reflectivity of wet

encrustation on sandstone was lower than that of dry encrustation. This may contribute to the increase of cleaning rate with water [8].

Cooper, et al. also found that the cleaning efficiency was enhanced in laser wet cleaning of limestone in terms of the removed encrustation area. The water could penetrate into the porous encrustation. During laser irradiation, the water in the pore would be explosively vaporized by the heat transferred from the encrustation, and generated large transit forces exerting on particles within the encrustation. These forces were sufficient to make the encrustation loose, which was very beneficial to laser cleaning [9]. However, the working mechanism of water in laser cleaning is still not very clear, and no any theoretical analysis has been done.

In the present paper, the mechanism of laser wet cleaning is proposed. Coupled heat and (moisture) mass transport within the laser irradiated porous encrustation is used to model laser wet cleaning. The corresponding governing equations are numerically solved with finite element methods to calculate the distribution of temperature, pressure and water volumetric fraction in the encrustation. The effects of distilled water, ethanol and acetone on the cleaning efficiency of the encrustation from marble are compared experimentally and numerically. There is some agreement between experimental and numerical values of the cleaning efficiency. Also, the color of marble surfaces cleaned by laser wet cleaning is analyzed.

Mechanism of Laser Wet Cleaning

In laser wet cleaning, the thin layer of liquid is sprayed onto the porous encrustation right before the laser irradiation. Liquid penetrates and fills in the minute pores of the encrustation. When laser irradiation starts, both the encrustation and liquid are heated. Once the temperature reaches the boiling point of liquid, liquid is vaporized immediately. Since liquid is vaporized at the rate much higher than its migration rate, the vapor pressure is built up in the pore. If the pressure is larger than the reduced tensile strength of the encrustation in the high temperature, the encrustation may be stripped away in the local area. The stripping in turn will accelerate the heat transfer in the encrustation and result in the new establishment of the pore pressure at the deeper level. Meanwhile, the ablation still plays a role in the removal of encrustation.

Mathematic Modeling

During laser wet cleaning, laser pulse induces the evaporation of liquid and the subsequent built-up of pressure in the pore. Driven by the pressure gradient, the liquid and the vapor are convected among the encrustation pores, which affect the heat transfer in the encrustation. Gypsum ($CaSO_4 \cdot 2H_2O$), the major encrustation ingredient, contains 21% chemically bound water by weight. Chemical bound water is released into the pore at 373 K and 573 K, respectively [10]. The absorbed laser heat is partly transferred into the encrustation by the liquid, vapor and encrustation together, partly absorbed by the evaporation of liquid, partly consumed by the gypsum dehydration. Accordingly, coupled heat transfer and mass transport determines the temperature and pressure distribution within the encrustation.

Coupled heat and mass transport in the porous encrustation is based on the averaging of the quantities over a representative elementary volume (REV) [11]. The volumetric fraction of each phase composing a REV with volume V is defined as

$$\varepsilon_i = \frac{V_i}{V}, i = s, l, g \quad (1)$$

where the subscripts *s, l, g* indicate solid, liquid, and gas, V_i is the phase i volume. The sum of the volumetric fractions of three phases is equal to 1. Suppose the porous encrustation is full of liquid before the irradiation. So, the encrustation porosity ε is denoted as $\varepsilon = \varepsilon_l + \varepsilon_g$ and $\varepsilon_s = 1 - \varepsilon$.

The following assumptions are applied. The liquid is incompressible, ρ_l = constant. Compared to the gas, the mobility of the liquid is negligible [12]. No dry air stays in the pore. The vapor phase is only liquid vapor. The vapor is the ideal gas. The encrustation is homogeneous and isotropic. The local thermodynamic equilibrium is achieved. Except dehydration of the gypsum, no other thermochemical reactions occur.

The mass conservation equation of gas is

$$\frac{\partial}{\partial t}(\rho_g \varepsilon_g) = -\nabla \cdot (\rho_g V_g) + \Gamma \quad (2)$$

where V_g is the gas velocity determined with Darcy's law as follows,

$$V = -\nabla \cdot (\frac{K}{\nu} P) \quad (3)$$

where K and ν is the permeability and dynamic viscosity of the vapor, and P is the pore pressure. Vapor density ρ_g is calculated with Dalton equation, $\rho_g = MP/RT$, where R is universal gas

constant, M is molar weight of vapor. Γ is the evaporation rate of liquid.

Based on the enthalpy balance, the heat conduction and convection in the encrustation is

$$\rho C_p \frac{\partial T}{\partial t} + \rho_g \varepsilon_g C_{pg} V \nabla T = \nabla \cdot (k \nabla T) \quad (4)$$

where T is temperature, t is time, ρC_p is the effective heat capacity for porous encrustation as $\rho C_p = (1-\varepsilon)\rho_s (C_{ps} + E\Delta h_d) + \varepsilon_l \rho_l (C_{pl} + F\Delta h) + \varepsilon_g \rho_g (C_{pg} + F\Delta h)$, where ρ_i and C_{pi} are density and specific heat of the corresponding phases, respectively [13]. Δh_d and Δh are the reaction heat of gypsum dehydration and the latent heat of the liquid vaporization, respectively. E and D are the derivative of solid and liquid phase volumetric fraction variation with temperature, respectively. The effective thermal conductivity for the porous encrustation k is defined as $k = (1-\varepsilon)k_s + \varepsilon_l k_l + \varepsilon_g k_g$ [14].

Only if the evaporation rate of liquid Γ is known, temperature, pore pressure and liquid volumetric fraction can be solved from equation (2) and (4). In the most coupled heat and mass transport models, a set of sorption isotherms is adopted to describe the dependence of water evaporation on temperature, pressure [12] [15]. The accurate sorption isotherms are rather difficult to be measured. Therefore, the evaporation rate of liquid is assumed to be related to the ratio of the vapor pressure to the saturated pressure at the corresponding temperature in some models [16-17]. However, such definition makes the accuracy of evaporation rate heavily rely on the estimated evaporation rate constant. In the present paper, taking the strong instantaneity of laser pulse into account, the vapor volumetric faction is defined as

$$\varepsilon_g = \varepsilon U(T - T_{trans}, \Delta T) \quad (5)$$

where U is a step function whose value is zero at $T \le T_{trans} - \Delta T$, equals to 1 at $T \ge T_{trans} + \Delta T$, and uniformly distributes in the range from T-T_{trans} to T+T_{trans} [18]. Therefore, one obtains that $\varepsilon_l = \varepsilon - \varepsilon_g$ and $D = U(T - T_{trans}, \Delta T) / dT$.

The encrustation porosity ε is varied with the dehydration of gypsum, like

$$\varepsilon = \varepsilon_0 + \frac{\rho_{water} \delta_{sw}}{\rho_s} \quad (6)$$

where ε_0 is initial porosity, the effective density of water ρ_{water} is 21% of water density, δ_{sw} is the released water fraction, defined like $\delta_{sw} = \xi U(T - T_{trans}, \Delta T)$, where U is also a step function, coefficient ζ is equal to 0.75 and 0.25 at T_{trans} of 373 K and 573 K, respectively. The encrustation density ρ_s is equal to $\rho_s = \rho_{s0} - \rho_{water} \delta_{sw}$, where ρ_{s0} is the initial encrustation density.

The initial conditions are assumed to be $T = 300K$, $P = 101325Pa = 1atm$, $\varepsilon_l = \varepsilon$, and $\varepsilon_g = 0$. On the laser-irradiated surface, the boundary condition is specified as $-K\nabla T \cdot \vec{n} = I + h(T - T_\infty)$, $P = 101325Pa = 1atm$, $\varepsilon_l = 0$ and $\varepsilon_g = \varepsilon$, where $\vec{n}$ is the outward unit vector of the surface, the heat transfer coefficient h is $h = h_c + \sigma e (T + T_\infty)(T^2 + T_\infty^2)$, where h_c is the convective heat transfer coefficient, σ is the Stefan-Boltzmann constant and e is the emissivity, T_∞ is the environment temperature of 300K. I is the absorbed laser fluence, like $I = \alpha I_0 \exp(-r^2 / b^2)$, where α is the surface absorptivity, I_0 is the incident fluence, b is the beam radius, r is the distance of the irradiated point to the beam center located at the symmetrical axis. On the non-laser-irradiated surface, the boundary conditions are applied, T = 300 K, $P = 101325Pa = 1atm$, $\varepsilon_l = 0$ and $\varepsilon_g = \varepsilon$.

Numerical Analysis

The coupled PDE equations (2) and (4) with boundary and initial conditions are solved through finite element methods. Software FEMLAB 3.2 is used. A two-dimensional axial symmetrical model with the dimension of 200μm×120μm is established. The mapped mesh with two-directional bias is created in the model, shown in Fig. 1. The application modes of transient conduction and convection, as well as Darcy's law in chemical engineering module are adopted.

In the model, a smoothed Heavyside function with a continuous second derivative, *flc2hs*, is chosen as the step function U. In the case of vaporized liquid (vapor), T_{trans} are set as 423 K, 401 K and 379 K for water, ethanol and acetone, respectively, and ΔT is 50 K. It is assumed that the water vaporizes starting from 373 K and all of water is vaporized at 473 K well below the critical point of water, 647K, because laser heating is extremely strong and fast. Similarly, the evaporation of ethanol and acetone is assumed to take place within the range from 351 K to 451 K and from 329 K to 429 K, respectively. Concerning gypsum dehydration, T_{trans} is

set as 398 K and 598 K for two dehydration reactions, respectively. And, ΔT is 25 K.

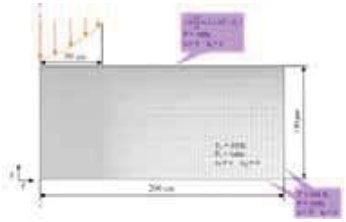

Fig.1 Schematic of the model for laser wet cleaning

Due to the constraint of the software, the part with the temperature reaching the vaporization point can not be removed from the calculation domain. To decrease its effect on the calculation results, the thermal conductivity in the ablated element is assumed to be 5000 once this element temperature is larger than the evaporation point.

All of thermodynamic data of liquids comes from [19]. Specific heat and dynamic viscosity of ethanol and acetone vapor are calculated with Method of Joback and Method of Chung, respectively [19]. In [20], the permeability of unfractured metamorphic rock is ranging from 10^{-18} to 10^{-20}. Marble belongs to metamorphic rock. However, the marble encrustation is mainly constituted by softer and water-soluble gypsum, so the porosity of encrustation gets larger. The permeability of the encrustation is assumed to be decreased to 1×10^{-12}.

Experimental Conditions and Material Characterizations

The studied sample is still Italian white Carrara marble with a honed surface. The sample is a cubic 15mm long, 15mm wide and 9mm thick. With the concern of numerical calculation accuracy, the marble is covered with the artificial encrustation, a compound of 5% hematite (Fe_2O_3) powder, 20% graphite powder and 75% gypsum (vol. %). The average encrustation thickness is approximately 120 microns. The formation method of the encrustation is introduced in details in [4].

Laser wet cleaning is performed with a Q-switched Nd:YAG laser at 355 nm in open air. The pulse duration is 50 ns. Other technical specifications of laser are given in [4]. All of cleaning experiments are conducted with the 100 μm laser beam. A thin layer of liquid is sprayed onto the encrustation every 2 seconds to assure the encrustation is wet. The compressed air is always blowing onto the focusing lens during cleaning. Thus, the focusing lens is protected from the attachment of ablated particles, but also the wet encrustation can not be blown dry.

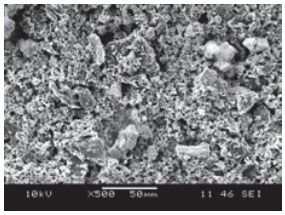

Fig. 2 SEM image of the artificial encrustation

SEM image of the encrustation presented in Fig. 2 reveals the artificial encrustation is the porous structure. Porosity measurement is based on Archimedes principle. The mixture including the same ingredients as the artificial encrustation is brushed onto the bottom of a 60 mm dish layer by layer, until reaching the thickness of 2.5 mm. This dish with the sample is weighed with the digital balance. Then, the distilled water is poured onto the sample surface very slowly to make sure the water fills in all of fine pores in the sample. The dish with the sample full of water is weighed again. Since the density of water is close to 1 kg/m^3, the ratio of the weight difference to the known sample volume is equal to the porosity of the sample.

The chromameter (Minolta CR-300) and surface enhanced Raman spectroscopy are employed to measure the surface color and constituents. Their detailed introductions are in [4]. SEM is used to take the image for the encrustation coated with silver.

Results and Discussions

Effect of Distilled Water on the Cleaning Efficiency

Experiments In the present paper, the cleaning efficiency is denoted as the weight of the encrustation removed by one single pulse. To increase the weight variation of the cleaned sample between pre- and pro-laser cleaning, a thin layer of encrustation in two circular areas with the diameter of 5 mm is removed. The laser pulses irradiate the encrustation along the circular orbits from the outside to the inside. The pulses have the overlapping rate of 50% to reduce the effect of the Gaussian beam. At the specified beam center locations, only one single pulse is deposited onto the encrustation. After two circular areas are irradiated once, the samples are weighed and compared with the initial weights. The sample weight difference divided by the number of deposited pulses, namely 16002, is equal to the ablated encrustation weight by

one single pulse. In laser wet cleaning, the cleaned samples are not weighed until they get dry.

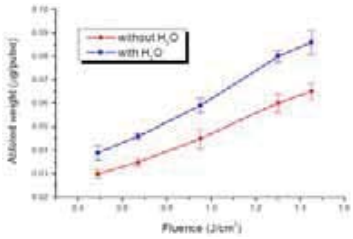

Fig. 3 The ablated weight by one single pulse at different fluence without and with distilled water

Considering the ablation thresholds of encrustation and marble at 355 nm, 0.45 J/cm^2 and 2.5 J/cm^2, respectively [4], the laser fluences of 0.49, 0.67, 0.95, 1.3, and 1.45 J/cm^2 are applied to ablate the encrustation without or with distilled water. The corresponding ablated encrustation weights by one single pulse are compared in Fig. 3. Obviously, the use of water enhances the cleaning efficiency at every fluence level. The white paper is put around the work stage during experiments to collect the encrustation debris. Some of debris shown in Fig. 4 is ranging approximately from 100 to 200 μm. These rather larger debris should be produced by the encrustation stripping due to the vapor pressure.

Fig. 4 Images of debris collected during experiment

In addition, Fig. 3 indicates the augment of the cleaning efficiency with the distilled water is enlarged with the fluence level. The possible reason is that the high fluence leads to high temperature and much stronger pressure. Moreover, the water in the deeper pores can be heated by the high fluence, and the vapor pressure is hence established there.

Simulated distribution of temperature, pressure and water volumetric fraction within the irradiated encrustation Assume that one single pulse at different fluences is shined on the encrustation. On the average, the measured porosity of the encrustation is approximately 0.475.

Figure 5 shows the surface contours of temperature, water volumetric fraction and pressure at 50 ns produced by the pulse at 0.67 J/cm^2 in the partial irradiated encrustation (10 μm × 98 μm). In the temperature contour, the red arrows denote the total heat flux. Two isotherm lines correspond to 2160 K and 373 K, respectively. The isotherm line of 2160 K is at the very shallow location, which means very few encrustation is thermally ablated. The isotherm line of 373 K indicates the water in the pores about 2.5 μm below the irradiated surface starts to vaporize. The distribution of water volumetric fraction agrees with the temperature contour. At temperature below 373 K, water fills in the pore, and the water volumetric fraction equates to the porosity of 0.475. At temperature above 373 k, all of water is vaporized in the majority of the area. Only the water in the very small area is within the evaporation.

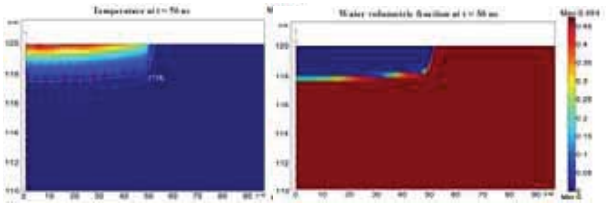

(a) (b)

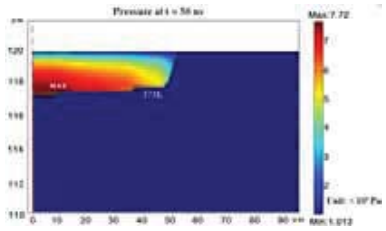

(c)

Fig. 5 Contours of (a) temperature with total heat flux, (b) water volumetric fraction and (c) pressure at 50 ns

The pressure contour shows the pressure is built up in the area at temperature above 373 k, encircled by the isotherm line of 373 K. In the area without water vaporization, the pressure is still equal to one atmosphere. The maximal pressure is marked. Obviously, its location is very near the start line of water vaporization. The pressure gradually decreases from the deep to the shallow area, which drives the water vapor to flow towards the encrustation surface and escape into the air. In addition, the maximal pressure approaches over 7.7 atm. Since the encrustation is artificially made, its tensile strength is assumed to be very low, approximately 3-4 atmosphere.

Accordingly, the maximal pressure may be large enough to spall the encrustation.

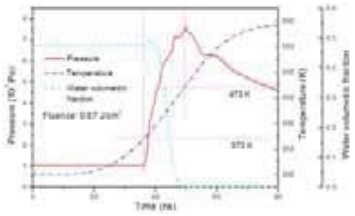

Fig. 6 History of temperature, pressure and water volumetric fraction at the maximal pressure point

The time history of temperature, pressure and water volumetric fraction at the point with the maximal pressure at 50 ns is shown in Fig. 6. At first 20 seconds, no absorbed laser heat is transferred to this point, and affects its temperature. Within the rest 30 seconds of the pulse duration, this point is heated. However, after 50 ns, its temperature continues to rise due to the heat from the top area with high temperature. Below 373 K, water volumetric fraction is equal to the porosity. Once the temperature reaching 373 K, water volumetric fraction increases a little bit due to the compromise of the vaporized water and the released water from the gypsum dehydration. Then, after the completeness of the gypsum dehydration, the variation of water volumetric fraction only reflects the extent of water vaporization. At 473 K, all of the water is vaporized.

The pressure starts to be built-up at 373 K. The peak value of pressure is located at the interface between the dry and wet encrustation with the temperature of 475 K. In addition, the pressure increases with the temperature during laser irradiation. The temperature still goes up after the laser irradiation, yet the pressure decreases. In the former case, the vaporization of more and more water is assigned to the pressure increase. In the latter case, the limited pressure increase due to the slow heating can not compensate the pressure decrease caused by the tempestuous gas movement upwards to the surface.

Figure 7 shows the time history of temperature and pressure at two points along the symmetrical axis with the depth of 0.1 and 1 μm, respectively. In Fig. 7(a), the point at the depth of 0.1 μm (z =119.9 μm) is heated up to 2160 K at approximately 35 ns. After 35 ns, its temperature fluctuates around 2160 K, which means this point is within the area thermally ablated. Concerning the point at the depth of 1 μm (z =119 μm), its temperature increase starts at about 7 ns and continues until 50 ns. After the end of pulse irradiation at 50 ns, its temperature keeps increasing for a little while due to the heat transferred from the above much hotter area, and then decreases. The model described in [4] is adopted to calculate the temperature produced at the same fluence as 0.67 J/cm^2 without the assistance of water. The corresponding temperature history at these two points is also shown in Fig. 7. It is obviously observed that the temperature produced without water is higher than that produced with water, which reflects water with the high specific heat cools down the encrustation.

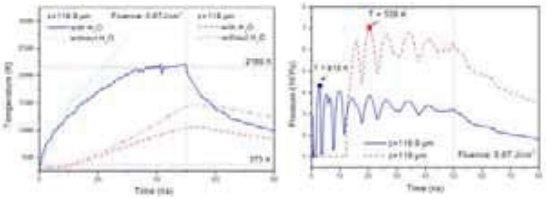

(a) (b)

Fig. 7 History of (a) temperature and (b) pressure of two points at the symmetrical axis

In Fig. 7(b), both the pressure at two points are established at 373 K. The pressure peaks of the points at 119 μm and 119.9 μm appear at 526 K and 815 K, respectively. Below 526 K and 815 K, the pressure is continuously increasing. Above 526 K and 815 K, the pressure gradually decreases.

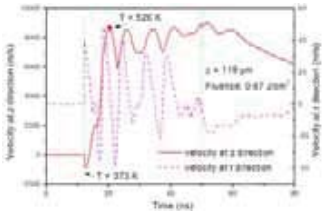

Fig. 8 History of vapor velocity of the point at the symmetrical axis (z = 119 μm)

The history of the velocities at the depth and radial direction of the point at z = 119 μm is presented in Fig. 8. The radial velocity is much smaller than the velocity at the depth direction. It can be reasoned that the convection of water vapor along the depth direction is much more intense due to the enormous pressure gradient along this direction. As vaporization starts, the negative vapor velocity at the depth direction represents the vapor moves downward due to its pressure lower than the pressure of the above nodes. Then, until 526 K or 815 K, the positive velocity means the newly formed vapor move upward from the liquid surface and is accumulated in the por. After that, the vapor starts to move out of the pore and towards the irradiated surface, which is verified by the positive velocity and the decreasing tendency of pressure.

The join of vapor escaped from the deeper pores enhances the pressure. On the other hand, the leaving of vapor further reduces the pressure. Accordingly, the pressure fluctuates and also leads to the fluctuation of the velocity. However, the velocity fluctuates around a constant value. This is because the fluctuating pressure decreases but the pressure gradient keeps constant. There is a noticeable fluctuation occurring at the rising phase of the pressure, shown in Fig. 7(b). Whereas, the velocity has not the corresponding fluctuation. The possible reason is the lower pressure is built-up during the initial water evaporation at the deeper level, as a result the partial vapor flowing downward causes this pressure fluctuation.

It can be seen in Fig. 7(b) that the pressure at 119 μm is always higher than that at 119.9 μm. The vapor in the shallow point is easy to escape, and then the pressure is hard to be built-up. What happens is opposite in the deep point.

Calculation of the ablated encrustation weight by one single pulse The pressure profiles along the symmetrical axis produced at the fluences of 0.49, 0.67, 0.95, 1.3, and 1.45 J/cm^2 at 50 ns are shown in Fig. 9. The pressure field extends with the fluence. The higher the fluence is applied, the larger the heat affected zone is generated. Therefore, more water reaches the boiling point, and then the pressure is built-up in the more area. As well, the induced maximal pressure increases with the fluence. At the high fluence, the water is vaporized much fast due to the high heating rate. Thus, the intensified amassment of the vapor promotes the boost of pressure.

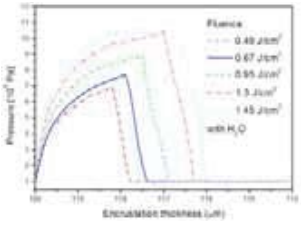

Fig. 9 Pressure profiles along the symmetrical axis at 50 ns produced by the different fluences

The pressure contours produced at 0.67 J/cm^2 at 10, 30 and 80 ns are shown in Fig. 10. It can be seen that the maximal pressure at 10, 30, 50 and 80 ns are about 6.5, 7.1, 7.7 and 4.9 atm, respectively. It can be seen that the maximal pressure appears at 50 ns during the whole laser wet cleaning. The increase of the generated maximal pressure with the heating time results from the difficulty of the vapor formed in the deeper level to flow out of the pore. At 80 ns, the heat transferred from the above hot area still can vaporize the water. Yet, the generated pressure is relatively low due to the slow heating rate.

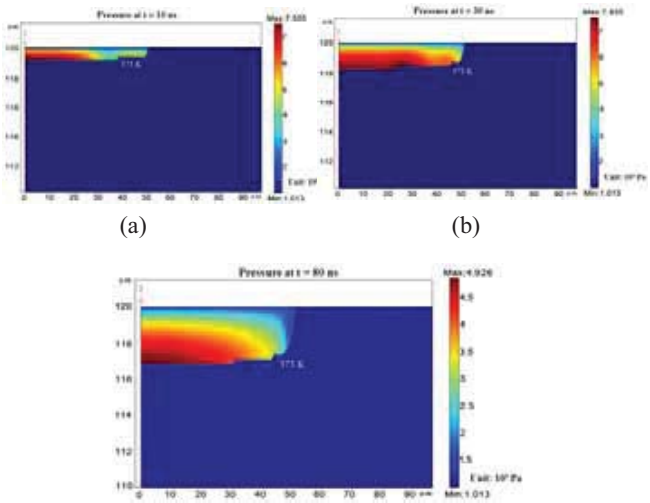

(a) (b)

(c)

Fig. 10 Contours of pressure at (a) 10 ns (b) 30 ns (c) 80 ns produced by the pulse at 0.67 J/cm^2

Suppose that once the maximal pressure at 50 ns exceeds the tensile strength, the whole encrustation with the diameter of 100 μm above the point with maximal pressure is completely removed. Accordingly, the ablated encrustation weight per pulse can be predicted. The experimental and simulated ablated encrustation weights by one single pulse are compared in Fig. 11. The simulated values have the same tendency as the experimental values. Also, the former is rather close to the latter. Therefore, the proposed model is validated by the experiments to some extent.

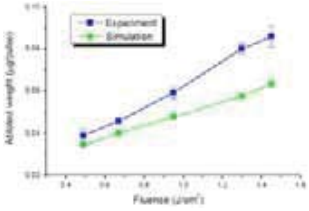

Fig. 11 Experimental and simulated ablated weight by one pulse at different fluence with distilled water

The discrepancy between the simulated and experimental ablated weights is due to the disadvantage of the present model. In the reality, a thin layer of encrustation may be stripped away at 10 ns due to the high pressure. Then, the laser beam is shined onto the newly exposed surface and establishes the pressure again. However, the present model can not

exclude the removed part from the calculation domain. The discrepancy is aggravated with the fluence, which further reflects the inappropriate treatment of the pressure-removed part because the enhanced pressure by the fluence plays a more important role. The future research will improve the model in this aspect.

Effect of Other Liquids on the Cleaning Efficiency

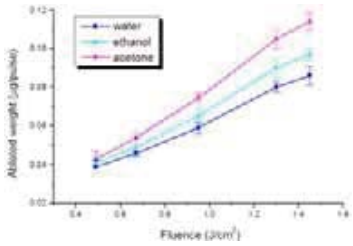

Fig. 12 Ablated weight by one single pulse at different fluence with different liquids

Liquids with the thermodynamic properties different from that of water affect the laser cleaning in a different way [21]. Ethanol and acetone are applied to assist the laser ablative cleaning. Both of them have very similar thermodynamic properties except that the boiling point and vaporization heat of ethanol are higher than that of acetone. However, their boiling point, specific heat, thermal conductivity and vaporization heat are lower than that of water.

To rather accurately determine the cleaning efficiency, the experimental strategy described in section 6.1.1 is followed. The laser cleaning with ethanol or acetone is performed at the fluence of 0.49, 0.67, 0.95, 1.3, and 1.45 J/cm^2, respectively. The ablated encrustation weight by one single pulse with distilled water, ethanol and acetone are compared in Fig. 12. At the same fluence, the ablated weight with acetone is the largest, that with distilled water is the smallest, and that with ethanol is in the middle. Though the ablated weight is enhanced with the fluence in all three cases, the increased values in the ablated weight with the acetone, ethanol and water are in the decreasing rank.

The simulated pressure profiles along the symmetrical axis produced at 0.67 J/cm^2 with distilled water, ethanol or acetone at 50 ns are compared in Fig. 13. Obviously, the vapor pressure is built-up in the deepest and widest area in the case of acetone. Its low thermodynamic data leads to that the heat is transferred much far and fast. Thus, acetone in much more pores is vaporized. In addition, the peak value of the pressure induced by acetone is largest partially due to the higher heating rate. The reason for the largest cleaning efficiency of acetone is likely explained.

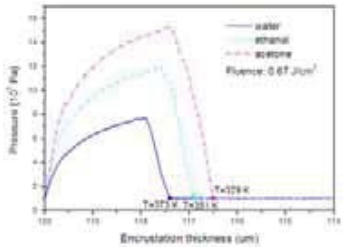

Fig. 13 Pressure profiles along the symmetrical axis at 50 ns with different liquids

Effect of Liquids on the Color of Cleaned Surface

To measure the surface color of cleaned marble, a circular encrustation with the diameter of 9 mm is removed to fit for the 8 mm measurement spot of the chromameter. The method to remove the circular encrustation is described in section 6.1.1. Zhang, et al. found that the marble surface became slightly yellowing after the cleaning with the 355 nm pulse at 0.67 J/cm^2 [4]. For the comparative analysis, the fluence of 0.67 J/cm^2 is applied to clean marble with liquids. The encrustation is completely removed by 8 pulses without liquids, 6 pulses with distilled water, 5 pulses with ethanol and 5 pulses with acetone, respectively. This also reflects the improvement in the cleaning efficiency of wet cleaning.

The color measurements of the original and cleaned marble surface are listed in Table 1. All of color data is the average of 5 independent measurements.

Four cleaned marble surfaces are very close to the original ones in the lightness, which implies the removal of the encrustation. The lightness difference between marble surface cleaned with liquids and the original surfaces is smaller than that between surface cleaned without liquids and its original surface. This means the encrustation may be completely removed in the former case. Without liquids, Δa^* of the cleaned surface is close to the original value and has the same sign. Yet, Δb^* of the cleaned surface is positive, which indicates the surface is becoming slightly yellowing. With liquids, both of Δa^* and Δb^* of the cleaned surfaces are close to the original values and have the same sign. It can be concluded that there is no discoloration on the surfaces cleaned at low fluence with liquids.

The Raman spectra activated on four cleaned surfaces at 514 nm are presented in Fig. 14. The

spectrum of the surface cleaned without liquids consists of bands of $CaCO_3$ at 158, 285, 711, 1084 cm^{-1} and bands of Fe_2O_3 at 224 and 405 cm^{-1} [4]. Yet, the spectra of the surface cleaned with liquids only have the bands of $CaCO_3$. The $CaCO_3$ bands in four spectra indicate the marble surfaces are exposed after the removal of the encrustation. The Fe_2O_3 bands reflect Fe_2O_3 still resides on the surface cleaned without liquids, responsible for the slightly surface yellowing.

Table 1 Color measurements of marble

	Initial	Cleaned	Initial	Cleaned + water
ΔL^*	90.8433	84.2767	84.9433	82.81667
Δa^*	-1.0333	-0.20333	-1.14267	-0.02823
Δb^*	-0.94	1.89333	-0.79167	-0.069
	Initial	Cleaned + ethanol	Initial	Cleaned + acetone
ΔL^*	85.1453	83.11822	87.071	84.0112
Δa^*	-0.98953	-0.05313	-1.1621	-0.0451
Δb^*	-1.09203	-0.0484	-1.12167	-0.07151
ΔL^*: Lightness; Δa^*: Red-Green; Δb^*: Blue-Yellow				

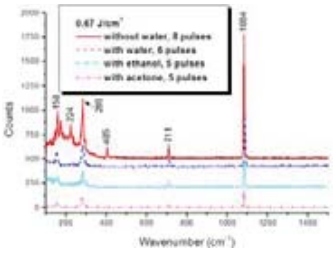

Fig. 14 Raman spectra of marble surface cleaned at $0.67J/cm^2$ without or with different liquids

In laser wet cleaning, since liquids consume the laser heat absorbed by the encrustation to raise the temperature and vaporize, the entire temperature field is decreased in the irradiated encrustation. This fact inhibits the reduction of hematite by the graphite. In addition, the majority of the encrustation is stripped away by the vapor pressure. The maximal vapor pressure takes place at the interface between the dry and wet encrustation, which is much lower than the ablation front in the encrustation. The stripping of the encrustation by the vapor pressure starts very near the interface. Even if some hematite is reduced into iron, the iron is taken away by the stripped encrustation, then can not reside and be oxidized by the air on the surface after the laser irradiation.

Conclusions

The enhanced cleaning efficiency of laser wet cleaning, in the case of the stone encrustation cleaning, is due to the generation of vapor pressure. The liquid in the encrustation pores is vaporized, and the accumulated vapor provokes the build-up of the pressure. Once the pore pressure exceeds the tensile strength of the encrustation, the encrustation is stripped away. The established model describing coupled heat transfer and mass transport in the porous structure can simulate the distribution of temperature, vapor pressure and liquid volumetric fraction in the encrustation produced by the laser irradiation. The model-predicted ablated encrustation weight by one single pulse agrees with the experimental values to some extent. The difference in the cleaning efficiency between laser wet and dry cleaning increases with the incident fluence. The use of the liquid with low boiling point and specific heat in laser wet cleaning is more beneficial to boost the cleaning efficiency. With the assistance of liquids, no discoloration occurs on the surface cleaned by the 355 nm pulse with the low fluence. The iron from the reduction of hematite by graphite is taken away by the pressure-induced removal of the encrustation.

Acknowledgement

The authors are grateful to Dr. Mohammad Athar and Dr. Xin Pei of Columbia University for the permission to access the chromameter and digital balance, respectively. The authors thank Mr. Justin Rasso for his technical assistance during the measurements.

References

[1] Asmus, J. F., Munk, W. & Murphy C. (1974) Studies on the interaction of laser radiation with art artifacts, Proceedings of the Society of Photo-Optical Instrumentation Engineers 4, 19-27.

[2] Siano, S., Fabiani, F., Pini, R., Salimbeni, R. Giamello M. & Sabatini, G. (2000) Determination of damage thresholds to prevent side effects in laser cleaning of pliocene sandstone of siena, J. Cult. Heritage 1, s47-s53.

[3] Klein, S., Fekrsanati, F., Hildenhagen, J, Dickmann, K., Uphoff, H., Marakis, Y. & Zafiropulos, V. (2001) Discoloration of marble during laser cleaning by Nd:YAG laser wavelengths, Appl. Surf. Sci. 171, 242-251.

[4] Zhang, J., Birnbaum, A. J., Yao, Y. L., Xu, F. & Lombardi, J. R. (2006) Effect of fluence on the

discoloration of marble cleaned with UV lasers, Appl. Surf. Sci., in press.

[5] Kim, D. & Lee, J. (2004) On the physical mechanism of liquid-assisted laser cleaning, J. Appl. Phys. 93(1), 762-764.

[6] Lu, Y. F., Song, W. D., Zhang, Y. & Low, T. S. (1998) Theoretical model and experimental study for dry and steam laser cleaning, Proc. of SPIE 3550, 7-18.

[7] Laboure, M., Bromblet, P., Orial, G., Wiedemann, G. & Simon-Boisson, C. (2000) Assessment of laser cleaning rate on limestones and sandstones, J. Cult. Heritage 1, s21-s27.

[8] Siano, S., Fabiani, F., Caruso, D., Pini, R. & Salimbeni, R. (2000) Laser cleaning of stones: assessment of operative parameters, damage thresholds and associated optical diagnostics, Proc. of SPIE 4070, 27-35.

[9] Cooper, M., Emmony, D. & Larson, J. (1995) Characterization of laser cleaning of limestone, Optics & Laser Tech. 27, 69-73.

[10] Thomas, G. (2002) Thermal properties of gypsum plasterboard at high temperature, Fire and Materials 26, 37-45.

[11] Whitaker, S. (1977) Simultaneous heat, mass and momentum transfer in porous media: a theory of drying, Advances in Heat Transfer 13, 119-200.

[12] Ahmed, G. & Hurst, J. (1997) Coupled heat and mass transport phenomena in siliceous aggregate concrete slabs subjected to fire, Fire and Materials 21, 161-168.

[13] Civan, F. & Sliepcevich, C. M. (1987) Limitation in the apparent heat capacity formulation for heat transfer with phase changes, Proc. Okla. Acad. Sci. 67, 83-88.

[14] Wei, C. K., Davis, H. T., Davis, E. A. & Gordon, J. (1985) Heat and mass transfer in water-laden sandstone: convective heating, AIChE Journal 31(8), 1338-1348.

[15] Ang, C. N. & Wang, Y. C. (2004) The effect of water movement on specific heat of gypsum plasterboard in heat transfer analysis under natural fire exposure, Construction and Building Materials 18, 505-515.

[16] Li, L. Y., Purkiss, J. A. & Tenchev, R. T. (2002) An engineering model for coupled heat and mass transfer analysis in heated concrete, J. Mech. Engi. Sci. 26, 213-224.

[17] Edmondson, P., Grammatika, M., Fryer, P. & Handy, B. (2005) Modelling of heat transfer, mass transfer and flavour development in chocolate crumb, Food and Bioproducts Processing 83(c2), 89-98.

[18] Civan, F., & Sliepcevich, C. M. (1987) Limitation in the apparent heat capacity formulation for heat transfer with phase changes, Proc. Okla. Acad. Sci. 67, 83-88.

[19] Reid, R., Prausnitz, J. M. & Poling, B. E. (1987) The Properties of Gases & Liquids, McGraw-Hill Book Company, New York.

[20] Hearst, J. R. & Nelson, P. H. (1985) Well Logging for Physical Properties, McGraw-Hill, New York.

[21] Lu, Y.F., Zhang, Y., Wan, Y.H. & Song, W.D. (1999) Laser cleaning of silicon surface with deposition of different liquid films, Appl. Surf. Sci. 138-139, 140-144.

Meet the Authors

Jie Zhang is a Ph.D candidate in the Department of Mechanical Engineering at Columbia University. B.S. and M.S. Xi'an Jiaotong University, China.

Andrew J. Birnbaum is currently a doctoral student in the Department of Mechanical Engineering at Columbia University. B.S and M.S. Carnegie Mellon University.

Y. Lawrence Yao is a Professor and chair in the Department of Mechanical Engineering at Columbia University. He received his Ph.D. from the University of Wisconsin-Madison in 1988. He serves on the Board of Directors of LIA.

Fen Xu is a Ph.D candidate in the Department of Chemistry at City College of New York. B.S. Wuhan University, China.

John R. Lombardi is a Professor in the Department of Chemistry at City College of New York. He received his Ph.D. from Harvard University in 1967.